

**Compression Molding Processed Superhydrophobic
CB/CeO₂/PVDF/CF Nanocomposites with Highly Robustness,
Reusability and Multifunction**

Binrui Wu^{a#}, Jiajie Lyu^{a#}, Chaoyi Peng^{a,b*}, Jun Liu^{a*}, Suli Xing^a, Dazhi Jiang^a,

Su Ju^a, Manish K. Tiwari^b

^aDepartment of Material Science and Engineering, College of Aerospace Science and Engineering, National University of Defense Technology, Changsha, Hunan, 410073, P. R. China

^bNanoengineered Systems Laboratory, UCL Mechanical Engineering, University College London, London, WC1E 7JE, UK

Abstract

Bioinspired superhydrophobic treatment imparts unique features to surfaces such as self-cleaning, water-proofing, anti-icing, anti-fouling, etc. Here we introduce a simple approach to manufacture carbon fiber based superhydrophobic nanocomposite materials. The developed materials had high mechanochemical durability and electrical conductivity which should find promising applications in many engineering fields. The nanocomposites were manufactured via molding process and comprised of carbon fiber (CF), poly(vinylidene fluoride) (PVDF), carbon black (CB) and cerium dioxide (CeO₂) nanoparticles, which is typically applied to fabricate carbon fiber reinforced plastics (CFRP) for structural use. The CFRP nanocomposites show a

* Corresponding author: chaoyi.peng@foxmail.com,

number of excellent functionalities such as superhydrophobicity (water contact angle $\sim 156^\circ$ and sliding angle $\sim 5^\circ$), excellent structural properties (tensile strength ~ 109 MPa and tensile modulus ~ 10 GPa) and electrical conductivity (~ 6.8 S/cm). The nanocomposites maintain excellent superhydrophobicity even after 200 cycles of sand paper abrasion, 24 hours of strong base and/or 60 min of strong acid erosion. Additionally, both the superhydrophobicity and mechanical properties can be recovered by re-molding process after the nanocomposites were cut into pieces or ground into powders. This demonstrates good reusability and clear potential for recycling of the developed materials.

Keywords: Nanocomposites; Superhydrophobicity; Reusability; Conductivity; Multifunction

1. Introduction

With a multitude of unique properties, such as self-cleaning [1-3], anti-icing [4], water-proofing [5] and anti-fouling [6], superhydrophobic materials with water contact angle (WCA) larger than 150° and water sliding angle (WSA) less than 10° [6-8] have attracted wide research interests. A variety of different techniques have been used to fabricate superhydrophobic surfaces, such as sol-gel [9,10], chemical vapor deposition [11], chemical etching [12,13], phase separation [14], electrochemical deposition [15], nanocomposite coatings [16,17]. Most of these works focused on introducing coatings or surface treatment on a substrate to create surface roughness as well as low surface energy, which are the two key factors for fabricating superhydrophobic materials [18-20]. However, such surface treatments face durability challenges due to the intrinsic fragile of nano-scaled surface roughness. Zhang et al. [21] created bulk superhydrophobic materials with durability, however, the mechanical properties of these composites and the electrical conductivity were relatively low.

Carbon fiber reinforced plastics (CFRP) are widely used as engineering structural materials to manufacture airplane wings, wind turbine blades, high-pressure containers, etc., due to their high specific strength and specific modulus [22-24]. However, the CFRP applications are often plagued by some nagging problems such as ice accretion (or icing), lightning and electrostatic [25-27]. More specifically, ice growth on the CFRP surface strongly affects the airfoils in airplane (the wings) and wind turbines (the blades) by reducing their aerodynamic performance, safety, and reliability [28, 29]; aircraft structures or some other electrical structures are sometimes subjected to

lightning strikes or electrostatic problems [30]. Rationally incorporating superhydrophobicity and electrical conductivity can help structural CFRP to overcome these shortcomings.

CFRP and carbon materials reinforced polymer nanocomposites have good mechanical properties [31-33], but they are much more expensive than traditional structural or engineering materials such as iron, aluminum and glass fiber composites etc. Furthermore, the castoffs of CFRP, including the off-cuts from manufacture process and end-of-life components, have reached a severe level [34]. The Landfill Directive (1999/31/EC) adopted by European Union in 1999 puts restraints on the landfilling of composite materials. Therefore, approaches to reuse these scrap materials are urgently required.

To address all the challenges above, in this work, a recyclable structural CFRP with superhydrophobicity and electrical conductivity was developed by adding rationally selected nanoparticles and via polymer composites fabrication protocols and molding process; and created a new class of nanocomposites by combining carbon black(CB), cerium dioxide (CeO_2), poly(vinylidene fluoride) (PVDF) and carbon fibers (CF) [35]. These nanocomposites not only possess mechanically and chemically durable superhydrophobicity, but also have good mechanical properties and electrical conductivity. The nanocomposites are also able to maintain the multifunctionality after being re-molded and re-shaped, thereby offering great potential for recyclability.

2. Experimental section

2.1 Materials

PVDF powders with number-average molecular weight of 100,000 g/mol were purchased from Slovey Co. Ltd. (USA). CeO₂ nanoparticles with average diameters of 100 nm were offered by Ganzhou Guangli Co. Ltd. (China). T300 carbon fiber plain weaves were supplied by Toray Co. Ltd. (Japan). Carbon fiber mat was purchased from Conmat Composite Factory. Carbon black (CB) we utilized is a specific kind, ketjen black EC-300J, which was purchased from KBIC Co. Ltd. (Japan). Dimethyl formamide (DMF), basic hydrochloric acid (HCl), sulfuric acid (H₂SO₄) sodium hydroxide (NaOH) and absolute alcohol were supplied by Huadong Reagent Factory (Shenzhen, China). Peel ply and poly(tetrafluoroethylene) (PTFE) film were ordered from Ruibide Composite Factory (China). Planetary ball mill was purchased from Tianchuang Co. Ltd. (Changsha China).

2.2 PVDF/CB/CeO₂ suspension preparation

Firstly, 70 g PVDF powder was added into 700 g N,N- Dimethylformamide (DMF) to form a uniform solution by magnetic stirring at 70 °C for 30 min. Then, 175 g CeO₂ powder and measured amounts of CB powder were dispersed into the PVDF solution and stirred for another 30 min. Finally, high speed shearer with a rotating speed of 10,000 rpm for 20 min to prevent the nanoparticles aggregating.

2.3 Fabrication of the CB/CeO₂/PVDF/CF impregnated superhydrophobic CFRP

The composites were fabricated by molding process, as shown schematically in Fig.1.

Firstly, two pieces of carbon fiber plain weaves, seven pieces of carbon fiber mats and

two pieces of peel plies were each cut to 360 mm × 360 mm size. Next, the fabrics were infused with the PVDF/CB/CeO₂ resin suspension by lay-up process to form the pre-impregnated (prepreg) sheets. Then, the prepreg was degassed by heating to 70 °C. Simultaneously, the steel mold (custom designed) was cleaned and prepped with a PTFE film to facilitate demolding. After that the prepreg was transferred into the prepared mold with two peel plies attached to each side of the prepreg and the mold was heated to 210 °C and compressed at 1 MPa for 1 hour. At last, the mold was cooled down to ambient temperature and the obtained nanocomposites were demolded.

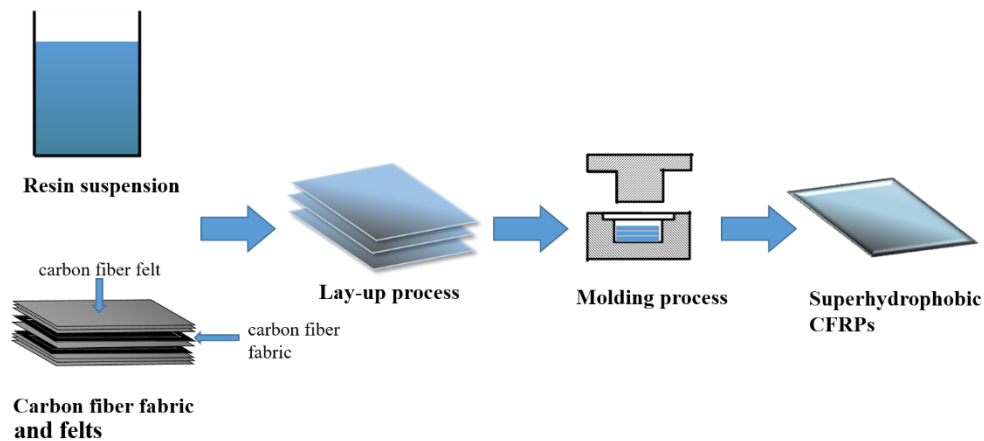


Fig. 1. Schematic illustration of fabrication process for superhydrophobic CFRP

2.4 Recycling the superhydrophobic CFRP

To demonstrate the feasibility of recycling or reusability, three different kinds of recycled superhydrophobic CFRP were fabricated (Fig. 2). To begin with, the scrap pieces – from the CB/CeO₂/PVDF/CF superhydrophobic CFRP with 5 g CB – were chopped into approximately 10 mm × 10 mm size pieces. For the first kind (Type A), mold was cleaned and covered with PTFE film to facilitate demolding. Then scrap CFRP pieces were then transferred to the mold and subjected to 220 °C temperature

under a pressure of 1 MPa for 1 hour. This was followed by cooling down and demolding. In the second approach (Type B), first a planetary ball mill was used to grind the scrap pieces into powder and mix them with extra PVDF powder. The purpose of the extra PVDF addition was to facilitate the molding process and assess the role of PVDF on wetting and mechanical properties (presented in Figs. 7 and 8 below). Next the scrap powder was shifted to the cleaned and PTFE film covered mold and heated to 220 °C under a pressure of 1 MPa for 1 hour. The resulting recycled sample was demolded after the mold cooled down to the ambient temperature. In the last recycling approach (Type C), DMF was added to the scrap pieces and a mixture was prepared through magnetic stirring on hot plate maintained at 70 °C until the resin completely dissolved. The resulting mixture was dried, cut into prepregs, followed by re-molding with the same molding procedures in section 2.3.

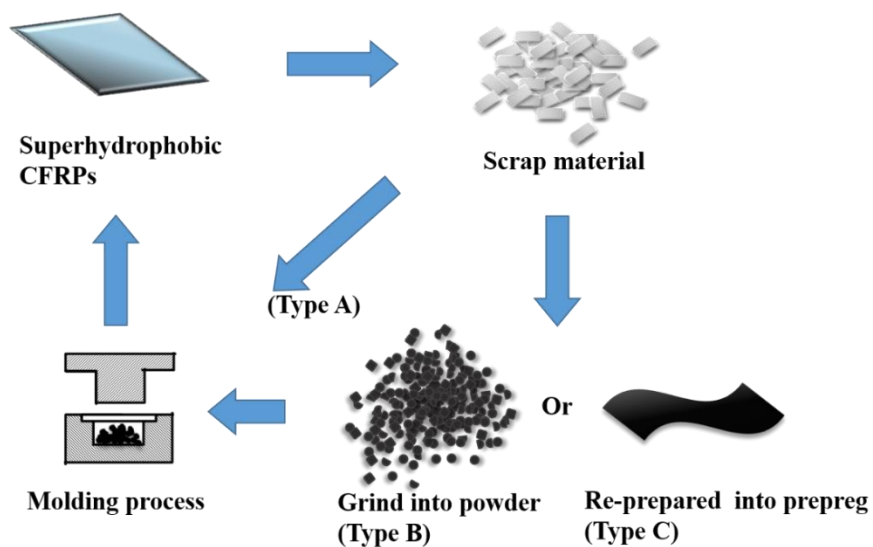


Fig. 2. Schematic illustration of recycling process for superhydrophobic CFRP

2.5 Characterization

The WCA was measured by a Contact Angle Meter (SL-200B, Shanghai Suolun Co.

Ltd.) with a 5 μL droplet of distilled water. Each reported WCA value is a mean of 5 measurements on different areas of the composite. The WSA measurements were acquired by gently dropping a 10 μL water droplets from slightly (~ 2 mm) above the composite surface maintained at specific tilt angle. WSAs were also measured at 5 different locations of each sample and averaged. The morphology of the composite was investigated using scanning electron microscopy (SEM) (Quanta-200, FEI Co. Ltd.).

Four probes tester (RTS-8, 4 probes tech Co. Ltd.) was used to measure the electrical conductivity of the composites, which was cut to round shapes with a 10 mm radius. The tensile strength and modulus of the samples were tested according to GB/T 3354-2014 standard, and those of the recycled samples were measured according to GB/T 1040.4-2008 standard. The surface composition was analyzed by X-ray photoelectron spectroscopy (XPS, Thermoelectron ESCALAB 250, USA). Various mechanical stability and chemical immersion tests were also performed to characterize the abrasion resistance, impact resistance and acid/base resistance of the nanocomposites.

3. Results and discussion

3.1 Morphology and surface composition

Figure 3 shows the SEM images of the PVDF/CF composites, CeO_2 /PVDF/CF composites and CB/ CeO_2 /PVDF/CF composites. The surface of the pristine PVDF/CF composites (Fig. 3a) is covered with interlaced carbon fibers, which are rather smooth (Fig. 3d). Overall, the surface is porous but without enough roughness which leads to a relatively low WCA of 108° . For the CeO_2 /PVDF/CF composites, the WCA is $\sim 152^\circ$

(Fig. 3b), indicating that rough structure of the CeO₂/PVDF on the carbon fibers can help trap air underneath a water droplet lying on the surfaces, which leads to the superhydrophobicity. The zoomed surface morphology is shown in Fig. 3e, clearly the surface possesses a rather smooth nanoscale roughness. Fig. 3c and 3f present the morphology of the CB/CeO₂/PVDF/CF composites, containing 2 wt.% CB. The surfaces are mainly covered with resin which show a rough microscale structure. Moreover, the higher magnification image in Fig. 3f shows that a large amount of nanospheres to be distributed on the surface. These nanoparticles together with microscale structures resulting from the particle clusters and the CFs assembly a micro/nano hierarchical structure. This hierarchical feature is markedly improved with CB addition (Fig. 3f) and contributes to the superior superhydrophobic property of the resulting nanocomposites.

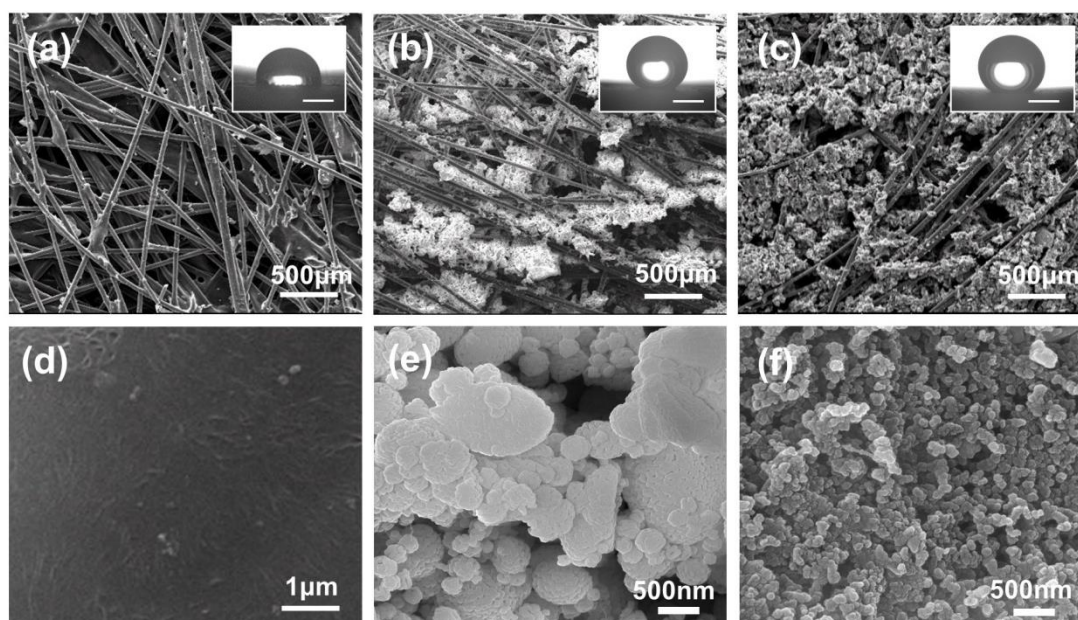


Fig. 3. SEM images of the composites at two different magnifications. (a, d) PVDF/CF composite, (b, e) CeO₂/PVDF/CF composite, (c, f) CB/ CeO₂/PVDF/CF composite with 2 wt.% CB. The insets in panels a-c show sessile water droplets on the surfaces

which were used for the contact angle measurements, the WCA values are 108° , 152° , 154° respectively; the scale bar in the inset droplet images is 1 mm.

Figure 4 shows the X-ray photoelectron spectroscopy (XPS) results of the CB/CeO₂/PVDF/CF nanocomposites (with 1 wt% CB). From the survey spectra (Fig. 4a), the elements C, O, F and Ce are detected. The high-resolution spectra O 1s, F 1s, C 1s and Ce 3d of the as-prepared sample are further illustrated in Figs 4b-e. The C 1s high-resolution spectrum (Fig. 4b) can be resolved into three components with binding energy of 284.6 eV, 286.1 eV and 291.1 eV. The strongest peak at 284.6 eV belongs to carbon fiber and the weak peaks 286.1 eV, 291.1 eV are assigned to PVDF [36-38]. The O 1s high-resolution spectrum (Fig. 4c) shows two major peaks at 529.6 eV and 532.5 eV, corresponding to CeO₂ and O atoms in carbon fiber [39,40]. Quantitative analysis of the XPS results reveal that the superhydrophobic surface consists of C (52.26 at%), O (17.71 at%), F (26.56 at%) and Ce (3.47 at%), which indicates that the surface is mainly built up by carbon fiber and PVDF.

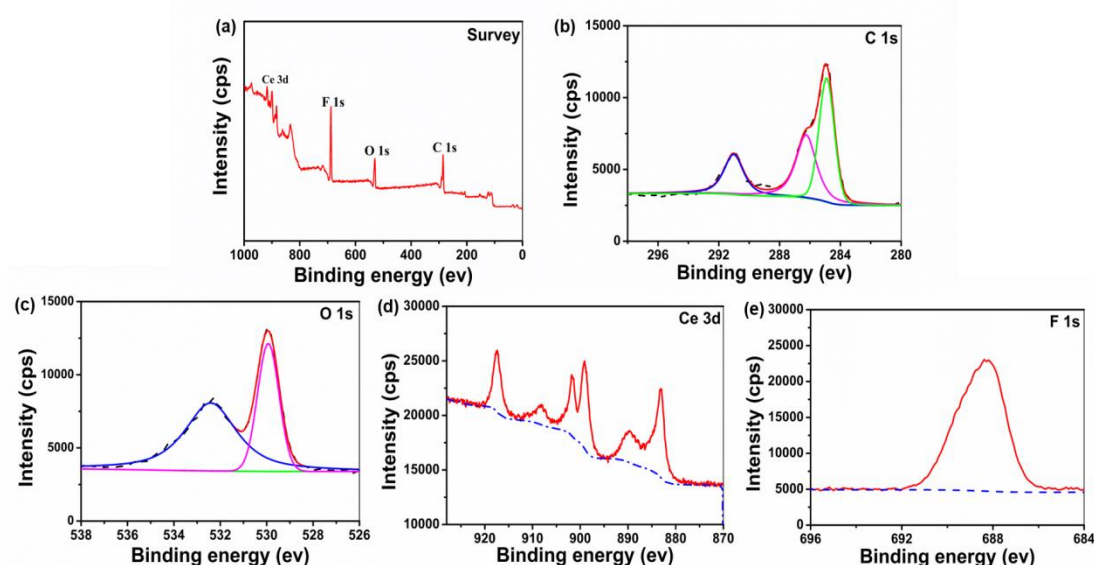


Fig. 4. (a) XPS survey spectra of CB/CeO₂/PVDF/CF nanocomposites; and XPS

high-resolution spectra: (b) C 1s, (c) O 1s, (d) Ce 3d and (e) F 1s.

3.2 Wettability and durability

Ketjen black, is a high conductivity carbon black (CB) with high specific surface area, branched structure and low surface energy [41]. It is widely used in fuel cells and electrochemical capacitors as carbon support [42]. In this work, carbon black was used to improve the superhydrophobicity as well as the electrical conductivity of the composite. The influence of CB content on the water wettability seems limited, as shown in Fig. 5a. With the increase of the CB content, WCA ascends mildly from 151° (without CB) to 156° (with 2 wt.% of CB). Simultaneously, the WSA reduces from 5° to 2°.

Compared to the wettability and hysteresis (WCA/WSA) measurements, droplet impact and bouncing offer stiffer test for liquid adhesion on superhydrophobic surfaces. Thus, the droplet impact and impalement resistance of our CB/CeO₂/PVDF/CF superhydrophobic composite were investigated using water droplet impacts. Liquid droplets with ~1.5 mm radius were impacted onto the composite from a height of 50 mm, and the whole process was recorded by the high-speed camera. The water drop showed complete rebound (Fig. 5b), which indicates that the CB/CeO₂/PVDF/CF composites possess superhydrophobic property. Superhydrophobicity hinders the water droplet from penetrating the surface texture [43-45] and a high receding contact angle ensures that surface energy in droplet at the maximum spreading stage is completely released during the droplet recoil [46], thereby leading to the droplet bouncing off. Eventually the bounced droplet falls back on the substrate and rests in a Cassie state –

we tested this by checking the roll off of the droplet after impact tests.

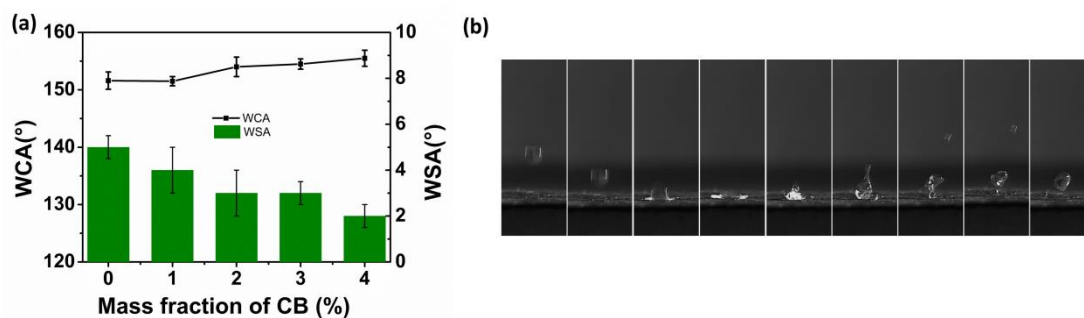


Fig. 5. (a) Effect of CB addition on the WCA and WSA. (b) Digitized images from the high-speed movies capturing the impact of water.

The chemical stability and mechanical durability of the superhydrophobic nanocomposites were evaluated. To assess chemical corrosion, we used 0.1M hydrochloric acid (HCl), sulfuric acid (H₂SO₄) and sodium hydroxide (NaOH) solutions. The tests were performed by immersing specimens into the chemical solutions and periodically removing the samples and measuring the WCA and WSA. As shown in Figure 6, the composites maintained superhydrophobicity after 60 min of 0.1M HCl (Fig. 6a) and H₂SO₄ (Fig. 6b) immersion, and after 24 hours of NaOH (Fig. 6c) immersion. The high chemical stability of the samples could be attributed to the excellent chemical inertness of PVDF and carbon fibers.

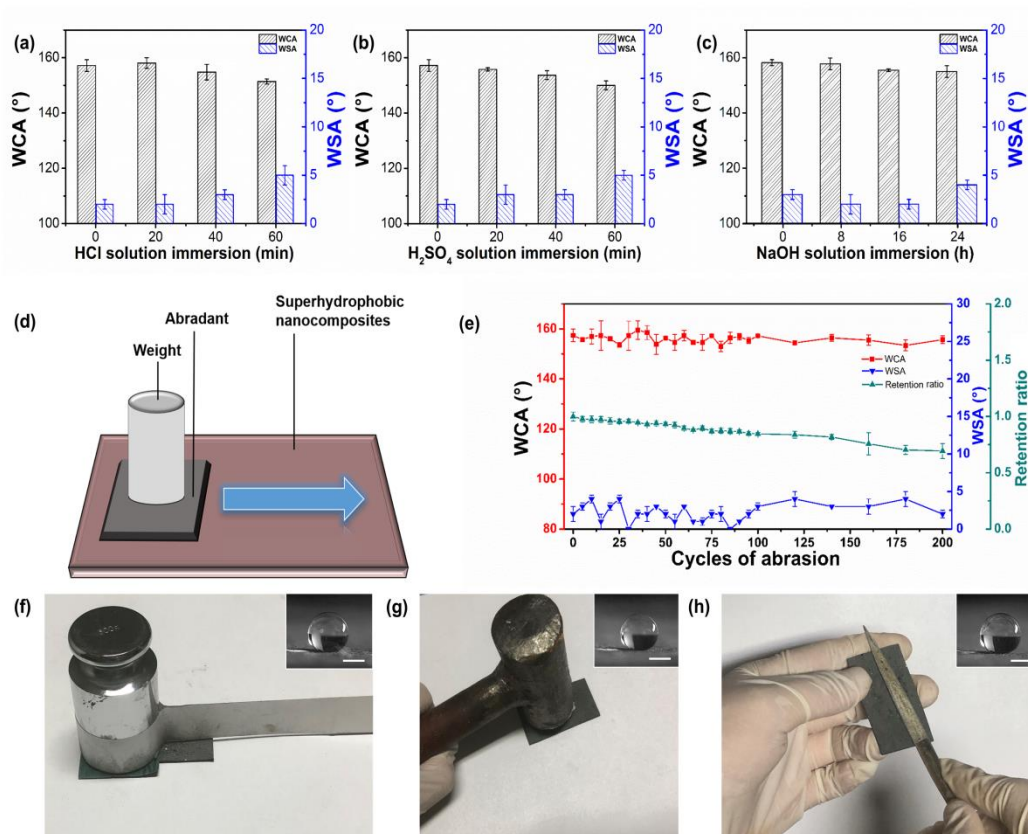


Fig. 6. Effect of (a) HCl (0.1M), (b) H₂SO₄ (0.1M) and (c) NaOH (0.1M) corrosion time on the wettability of CB/CeO₂/PVDF/CF superhydrophobic CFRP. (d) Schematic illustration of abrasion test for the CB/CeO₂/PVDF/CF superhydrophobic CFRP. (e) Effect of abrasion cycles on the wettability of the superhydrophobic CFRP. (f) – (h) mechanical tests on the CB/CeO₂/PVDF/CF superhydrophobic CFRP. (f) Sand paper abrasion. (g) Hammer beat test. (h) File abrasion test in air. Inserts show the wettability of the sample after the corresponding tests; each inset scale bar is 1 mm.

To determine the mechanical stability of the superhydrophobic nanocomposites, a series tests were carried out. Figure 6d and 6f show the sandpaper abrasion test setup in schematic and photo, respectively. A sandpaper with grit 600 was employed as abradant to closely sand the surface (also see movie S1). The abradant was driven to move along the surface with a load of 500g on it. To further quantify the abrasion resistance, WCA,

WSA and retention ratio were measured as a function of the abrasion cycles; the results are plotted in Fig. 6e. The retention ratio is calculated as $\eta = h_1/h_2 \times 100\%$, where h_1 , h_2 refers to the abraded sample thickness and original sample thickness, respectively. After 200 cycles of abrasion, the WCA declined to $153.8^\circ \pm 1.1^\circ$, with a WSA of $2.0^\circ \pm 0.5^\circ$ and retention ratio of 0.69 ± 0.06 , still maintaining good superhydrophobicity. In addition, we performed iron hammer beat test and file abrasion test on the surface in the air to demonstrate the nanocomposites maintain superhydrophobicity (see Fig. 6g-h and Movie S2-3). Overall, these tests clearly indicate that our superhydrophobic nanocomposites have good mechanical robustness, which is important in practical applications.

3.3 Mechanical properties and conductivity

The mechanical properties of composites are markedly influenced by the lay-up designs. In a symmetric structure, two carbon fiber plain weaves and a carbon fiber mat were in the middle, and three pieces of carbon fiber mats were each added from top and bottom. Overall, seven pieces of CF mats and two pieces of CF weaves were used, each being $360 \text{ mm} \times 360 \text{ mm}$ in size. The resulting lay-up was soaked in resin and molded just as described above in Section 2.3. The mechanical property of the resulting composite was evaluated by measuring their tensile strength and modulus. The nominal sizes of the test specimens were $250 \text{ mm} \times 25 \text{ mm} \times h \text{ mm}$, with h being the composite thickness. The main goal here was to understand the effect of CB addition on the tensile mechanical properties.

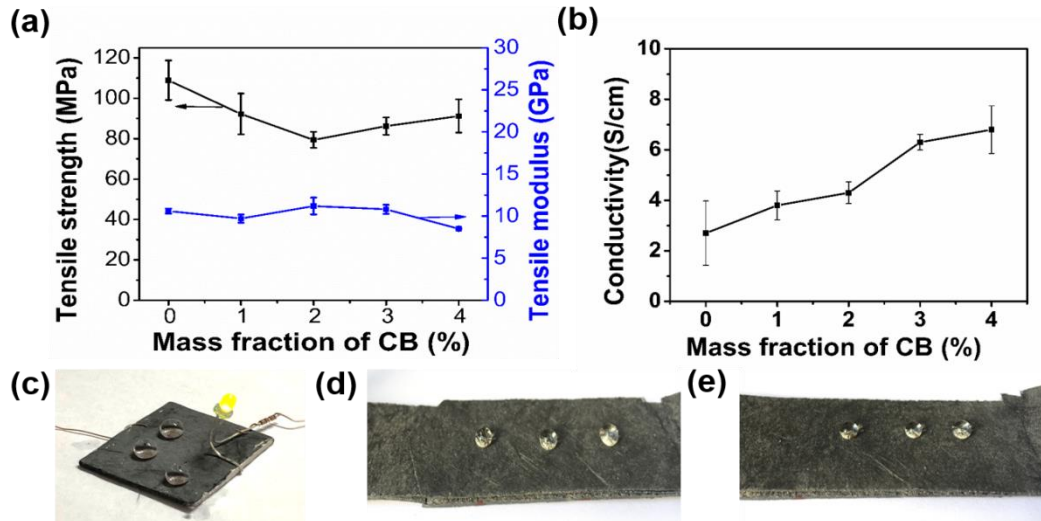


Fig. 7. The effect of CB addition on tensile strength, modulus (a) and conductivity (b). (c) Optical images of water drops beaded on the surface demonstrating electrical conductivity and superhydrophobicity (d-e) Optical images of water droplets lying on the delaminated interfaces of the CB/CeO₂/PVDF/CF nanocomposites, showing superhydrophobicity across the composite layer

With initial increase in CB content (< 2%), the tensile strength of the nanocomposite dropped appreciably, from 108.9 MPa to 79.4 MPa (Fig. 7a). However, upon further increase in CB the strength partially recovered to 91.2 MPa. The tensile modulus on the other hand (Fig. 7a) of the nano-composites is all around 10 GPa without statistic difference. This indicates that CB addition causes a rather small influence (about 10% between the highest and lowest) to the stiffness of the composite, as the stiffness of the composites mainly stems from CFs.

The effect of CB content on the composite electrical conductivity is plotted in Fig. 7b. With the increase of CB addition, conductivity rose from 2.7 S/cm to 6.8 S/cm, which is attributed to the high electrical conductivity of CB. Also, the superhydrophobicity and conductivity are demonstrated simultaneously by beaded water drops, which slid of the

surfaces readily, and the lit up LED (see Fig. 7c and Movie S4). Interestingly, after the tensile test, the interfaces between different layers, were found to retain superhydrophobic property. Figure 7d-e show optical images of the water droplets on the different interfaces of the chapped interface. The high contact angle of the droplets clearly attests the superhydrophobic nature of the layers of the nanocomposites.

3.4 Reusability and recyclability

The thermoplastic CFRP composites presented here are expected to be recyclable. To demonstrate this, three different methods as depicted in Fig. 2 were used to manufacture recycled nanocomposites. Type A samples were prepared by molding scrap pieces directly, Type B by molding the powder form of scrap and Type C by re-dissolving the scrap in DMF followed by casting, prepreg preparation and molding.

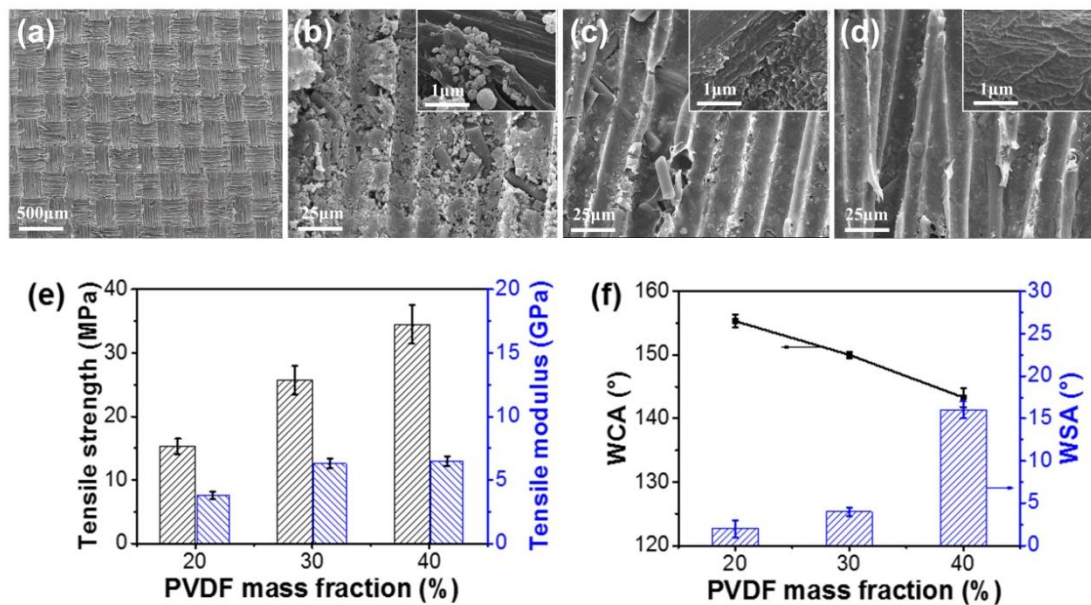


Fig. 8. (a) SEM image capturing the morphology of a Type B sample with 20 wt.% PVDF, and magnified images with different Type B samples with varying PVDF content: 20 wt.%(b), 30 wt.% (c) and 40 wt.% (d). The effect of PVDF content on tensile strength and modulus (e) and WCA and WSA (f) of the Type B recycled CFRP.

The inserts in panels b, c, and d are magnified surface morphology of each surfaces.

Figure 8 shows the tensile results for Type B samples. Figures 8a-d show the morphology of the Type B samples. Firstly, Fig.8a shows a large-area view for a sample with 20 wt.% PVDF; in fact, all three samples share a similar surface structure. The surface clearly shows regular tetragonal pattern consistent with mold texture. To study the morphology more closely, higher resolution images were obtained from inside the individual tetragonal units and are shown in Figs. 8b-c. These zoomed-in images clearly show the microscale line arrays consistent with presence of carbon fibers in the composite. Furthermore, for the sample with 20 wt.% PVDF (Fig.8b), the surface exhibits a porous structure comprising nanoscale pores. These nanopores together with microscale grooves form an ideal hierarchical nano-micro structure that can facilitate the superhydrophobicity. With increase in the PVDF content (Figs. 8c and d), the surfaces become close-grained and smooth without nanoscale structure. The results of the corresponding mechanical properties and wettability tests are presented in Figs. 8e and f, respectively. With the increase in the PVDF content, the tensile strength rises from 15.3 MPa to 34.2 MPa (Fig. 8e). The tensile modulus also rises from 3.8 GPa to 6.5 GPa, but the differences between the modulus of composites with 30 wt.% PVDF and 40 wt.% PVDF is negligible. As for the wettability of the samples (Fig. 8f), the WCA falls from 155° (PVDF 20 wt.%) to 143° (PVDF 40 wt.%) and WSA increases from 2° to 16°. The dissimilarity of the morphology noted above can explain the reduction in the contact angle, rise in hysteresis as well as the improvement of the tensile mechanical properties. The micro/nano hierarchical structure accounts for the

superhydrophobicity of the recycled samples with 20 wt.% PVDF. However, the nanopores weaken samples through stress concentration, which is reflected in the reduced tensile strength. On the other hand, the smooth surfaces show reduced non-wetting (contact angle) but improved tensile strength, as less nano-voids are present.

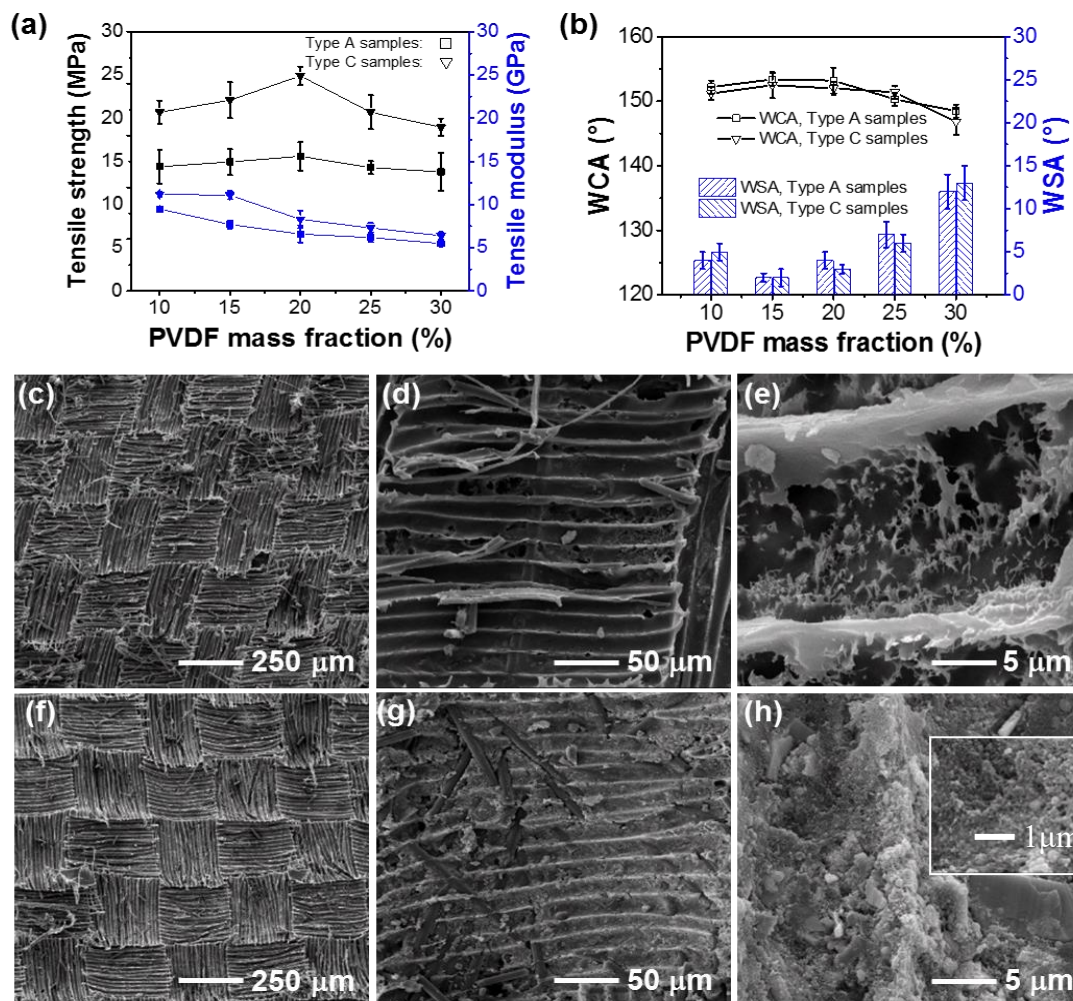


Fig. 9. Effect of PVDF contact on tensile strength and modulus (a) and WCA and WSA for Type A and C samples (b). SEM images at low (c) and high magnifications (d-e) of a Type A samples with 20 wt.% PVDF showing the overall morphology and detailed micro/nanoscale morphology features. Low (f) and high magnification (g-h) SEM images of Type C samples with 20 wt.% PVDF.

The results of mechanical testing, wettability and morphological assessment on Type A and C specimens are shown in Figure 9. Firstly, role of PVDF content on tensile strength and modulus is plotted in Fig. 10a, where both Type A and C samples show similar trends. In both cases, the tensile strength increases from 10 wt.% to 20 wt.% of PVDF, and then declines moderately upon further increase in PVDF content. However, the tensile strength of C samples is 10 MPa larger than the A sample counterparts, with the maximal value reaching 41.2 MPa. The tensile modulus of both type of samples broadly have a decreasing trend with PVDF content increasing, with the modulus of Type C samples being higher than that of the Type A. As for the wettability (Fig. 9b), the WCA values of A and C samples are nearly identical within the measurement error, with sample containing > 20 wt.% PVDF show slight decline in the contact angle. The reason for this is reduction in surface roughness reduction with PVDF content, which is similar to what was found for Type B samples. The roughness reduction is also reflected in progressive rise in WSA with increase in the PVDF content (Fig. 9b).

The morphology of A and C samples with 20 wt.% of PVDF are presented in Figs. 9c-h. Overall structures are similar for both samples types (Fig. 9c and f); however, the higher magnification images clearly show that carbon fibers are distributed more uniformly in C sample. The mis-oriented carbon fibers in A sample creates more defects, hence leading to lower tensile strength than that of C sample. Additionally, Figs. 9e-h show that for both sample types, the morphology contains micro-nano hierarchical structures that facilitates superhydrophobicity (c.f. Fig. 9b).

4. Conclusion

In this work, we fabricated a new class of reusable, multifunctional nanocomposites by molding process with ingredients of CB, PVDF, CF plain weave, CF mat and CeO₂ nanoparticles. Comparing with pristine CF/PVDF composites, CeO₂ particles endow the composites with superhydrophobicity. The addition of CB could improve the wettability of the composites as well as the conductivity (from 2.7 S/cm to 6.8 S/cm), this should exhibit very good anti-electrostatic and anti-lightning performances comparing with most polymer composites. These multifunctional nanocomposites also show good chemical and mechanical robustness, which could sustain superhydrophobicity after 200 cycles of sanding abrasion, and 24 hours of strong base or 60 min of acid immersion. The mechanical properties of these multifunctional nanocomposites are superior to most bulky plastics by tensile strength of 99.2 MPa and tensile modulus of 10 GPa, which would allow them to serve as structural materials. Furthermore, the composites could be reused in three different ways, which still possesses good water repellence and mechanical property after reusable treatment. Thus, these multifunctional nanocomposites will find potential applications in structural engineering with additional requirements for non-wetting, water-proofing, self-cleaning, anti-fouling and anti-electrostatic.

5. Notes

The authors declare no competing financial interest.

Acknowledgements

The research was supported by the National Natural Science Foundation of China

(No. 51203183 and No. 51403235). MKT Acknowledges support from EPSRC First Grant EP/N006577/1.

References

- [1] Varshney P, Mohapatra S S. Durable and regenerable superhydrophobic coatings for brass surfaces with excellent self-cleaning and anti-fogging properties prepared by immersion technique[J]. Tribology International, 2018, 123: 17-25.
- [2] Wu Y, Shen Y, Tao J, et al. Facile spraying fabrication of highly flexible and mechanically robust superhydrophobic F-SiO₂@ PDMS coatings for self-cleaning and drag-reduction applications[J]. New Journal of Chemistry, 2018, 42(22): 18208-18216.
- [3] Junyan Peng, Xiujian Zhao, Wufeng Wang, et al. Durable Self-Cleaning Surfaces with Superhydrophobic and Highly Oleophobic Properties[J]. Langmuir, 2019, 35(25).
- [4] Yang Wenxuan, Yuan Yuan, Liu Guoyong, et al. The anti-icing/frosting aluminum surface with hydrangea-like micro/nano structure prepared by chemical etching[J]. Materials Letters, 2018, 226.
- [5] Lu, Yao, Sathasivam, Sanjayan, Song, Jinlong, et al. Creating superhydrophobic mild steel surfaces for water proofing and oil–water separation[J]. Journal of Materials Chemistry A, 2014, 2(30):11628.
- [6] Kong X, Zhang J, Xuan Q, et al. Superhydrophobic coating for antifouling of Chinese paintings[J]. Langmuir, 2018, 34(28): 8294-8301.
- [7] Victor JJ, Facchini D, Erb U. A low-cost method to produce superhydrophobic polymer surfaces. Journal of Materials Science 2012; 47: 3690-3697.
- [8] Shahsavan H, Arunbabu D, Zhao B. Biomimetic modification of polymeric surfaces: a

promising pathway for tuning of wetting and adhesion. *Macromolecular Materials & Engineering* 2012; 297: 743–760.

[9] Yang M, Liu W, Jiang C, et al. Fabrication of superhydrophobic cotton fabric with fluorinated TiO₂ sol by a green and one-step sol-gel process[J]. *Carbohydrate polymers*, 2018, 197: 75-82.

[10] Czyzyk S, Dotan A, Dodiuk H, et al. Easy-to-Clean Superhydrophobic Coatings Based on Sol-Gel Technology: A Critical[J]. *Progress in Adhesion and Adhesives*, 2018: 307.

[11] Crick CR, Bear JC, Kafizas A, Parkin IP. Superhydrophobic photocatalytic surfaces through direct incorporation of titania nanoparticles into a polymer matrix by aerosol assisted chemical vapor deposition. *Advanced Materials* 2012; 24: 3505-8.

[12] Saleh T A, Baig N. Efficient chemical etching procedure for the generation of superhydrophobic surfaces for separation of oil from water[J]. *Progress in Organic Coatings*, 2019, 133: 27-32.

[13] Jung S, Tiwari MK, Doan NV, Poulidakos D. Mechanism of supercooled droplet freezing on surfaces. *Nature Communications* 2012; 3: 299-306.

[14] Seyfi J, Panahi-Sarmad M, OraeiGhodousi A, et al. Antibacterial superhydrophobic polyvinyl chloride surfaces via the improved phase separation process using silver phosphate nanoparticles[J]. *Colloids and Surfaces B: Biointerfaces*, 2019, 183: 110438.

[15] Xue Y, Wang S, Zhao G, et al. Fabrication of NiCo coating by electrochemical deposition with high super-hydrophobic properties for corrosion protection[J]. *Surface and Coatings Technology*, 2019, 363: 352-361.

- [16] Feng Y, Peng C, Li Y, et al. Superhydrophobic nanocomposite coatings with photoinitiated three-dimensional networks based on reactive graphene nanosheet-induced self-wrinkling patterned surfaces[J]. *Journal of colloid and interface science*, 2019, 536: 149-159.
- [17] Bolvardi B, Seyfi J, Hejazi I, et al. Towards an efficient and durable superhydrophobic mesh coated by PDMS/TiO₂ nanocomposites for oil/water separation[J]. *Applied Surface Science*, 2019, 492: 862-870.
- [18] Latthe S S, Sutar R S, Bhosale A K, et al. Superhydrophobic surfaces for oil-water separation[M]//*Superhydrophobic Polymer Coatings*. Elsevier, 2019: 339-356.
- [19] Milionis A, Sharma C S, Hopf R, et al. Engineering fully organic and biodegradable superhydrophobic materials[J]. *Advanced Materials Interfaces*, 2019, 6(1): 1801202.
- [20] Latthe S S, Sutar R S, Kodag V S, et al. Self-cleaning superhydrophobic coatings: Potential industrial applications[J]. *Progress in Organic Coatings*, 2019, 128: 52-58.
- [21] Zhang X, Zhi D, Sun L, et al. Super-durable, non-fluorinated superhydrophobic free-standing items. *Journal of Materials Chemistry A*, 2017.
- [22] Kirchdoerfer T, Liebscher A, Ortiz M. CTH shock physics simulation of non-linear material effects within an aerospace CFRP fastener assembly due to direct lightning attachment[J]. *Composite Structures*, 2018, 189: 357-365.
- [23] Geier N, Davim J P, Szalay T. Advanced cutting tools and technologies for drilling carbon fibre reinforced polymer (CFRP) composites: a review[J]. *Composites Part A: Applied Science and Manufacturing*, 2019: 105552.
- [24] Al-Salloum Y A, Al-Amri G S, Siddiqui N A, et al. Effectiveness of CFRP Strengthening

in Improving Cyclic Compression Response of Slender RC Columns[J]. Journal of Composites for Construction, 2018, 22(3): 04018009.

[25] Maleki P, Iranpour B, Shafabakhsh G. Investigation of de-icing of roads with conductive concrete pavement containing carbon fibre-reinforced polymer (CFRP)[J]. International Journal of Pavement Engineering, 2019, 20(6): 682-690.

[26] Hung P, Lau K, Fox B, et al. Effect of graphene oxide concentration on flexural properties of CFRP at low temperature[J]. Carbon, 2019.

[27] Wang Z, Xian G, Zhao X L. Effects of hydrothermal aging on carbon fibre/epoxy composites with different interfacial bonding strength[J]. Construction and Building Materials, 2018, 161: 634-648.

[28] Gao L, Liu Y, Zhou W, et al. An experimental study on the aerodynamic performance degradation of a wind turbine blade model induced by ice accretion process[J]. Renewable energy, 2019, 133: 663-675.

[29] Raj L P, Lee J W, Myong R S. Ice accretion and aerodynamic effects on a multi-element airfoil under SLD icing conditions[J]. Aerospace Science and Technology, 2019, 85: 320-333.

[30] Tailliet F. Structure for protecting an integrated circuit against electrostatic discharges: U.S. Patent Application 15/436,819[P]. 2018-2-1.

[31] Zare Y, Rhee K Y. Following the morphological and thermal properties of PLA/PEO blends containing carbon nanotubes (CNTs) during hydrolytic degradation[J]. Composites Part B: Engineering, 2019, 175: 107132.

[32] Razavi R, Zare Y, Rhee K Y. The roles of interphase and filler dimensions in the properties of tunneling spaces between CNT in polymer nanocomposites[J]. Polymer

Composites, 2019, 40(2): 801-810.

[33] Zare Y, Park S P, Rhee K Y. Analysis of complex viscosity and shear thinning behavior in poly (lactic acid)/poly (ethylene oxide)/carbon nanotubes biosensor based on Carreau–Yasuda model[J]. Results in Physics, 2019, 13: 102245.

[34] Shen L, Ding H, Cao Q, Jia W, Wang W, Guo Q. Fabrication of ketjen black-high density polyethylene superhydrophobic conductive surfaces. Carbon 2012; 50: 4284-4290.

[35] Choolaei M, Goodarzi V, Khonakdar H A, et al. Influence of graphene oxide on crystallization behavior and chain folding surface free energy of poly (vinylidene fluoride-co-hexafluoropropylene)[J]. Macromolecular Chemistry and Physics, 2017, 218(19): 1700103.

[36] Li M, Shi J, Chen C, et al. Optimized permeation and antifouling of PVDF hybrid ultrafiltration membranes: synergistic effect of dispersion and migration for fluorinated graphene oxide[J]. Journal of Nanoparticle Research, 2017, 19(3): 114.

[37] Liu D, Li D, Du D, et al. Antifouling PVDF membrane with hydrophilic surface of terry pile-like structure[J]. Journal of Membrane Science, 2015, 493: 243-251.

[38] Zhang Z, Wu X, Wang L, et al. Wetting mechanism of a PVDF hollow fiber membrane in immersed membrane contactors for CO₂ capture in the presence of monoethanolamine[J]. RSC Advances, 2017, 7(22): 13451-13457.

[39] Yu G, Han K, Wang J, et al. Steam-treated CeO₂-ZrO₂/activated carbon fibers for the efficient removal of Pb (II) from aqueous solutions[J]. Colloids and Surfaces A: Physicochemical and Engineering Aspects, 2019, 566: 29-37.

[40] Kunitomo H, Ishitobi H, Nakagawa N. Optimized CeO₂ content of the carbon nanofiber

support of PtRu catalyst for direct methanol fuel cells[J]. *Journal of Power Sources*, 2015, 297: 400-407.

[41] Qian X, Jin L, Zhu L, et al. CeO₂ nanodots decorated ketjen black for high performance lithium–sulfur batteries[J]. *RSC Advances*, 2016, 6(112): 111190-111196..

[42] Richard D, Clanet C, Quéré D. Contact time of a bouncing drop. *Nature* 2002; 417: 811-811.

[43] Deng X, Mammen L, Butt HJ, Vollmer D. Candle soot as a template for a transparent robust superamphiphobic coating. *Science* 2011; 335: 67-70.

[44] Maitra T, Tiwari MK, Antonini C, Schoch P, Jung S, Eberle P, et al. On the nanoengineering of superhydrophobic and impalement resistant surface textures below the freezing temperature. *Nano Letters* 2014; 14: 172-82.

[45] Antonini C, Villa F, Bernagozzi I, Amirfazli A, Marengo M. Drop rebound after impact: the role of the receding contact angle. *Langmuir* 2013; 29: 16045-16050.

[46] Maitra T, Antonini C, Tiwari MK, Mularczyk A, Imeri Z, Schoch P, et al. Supercooled water drops impacting superhydrophobic textures. *Langmuir the Acs Journal of Surfaces & Colloids* 2014; 30: 10855-61.